36th AIAA Plasmadynamics and Lasers Conference
6-9 June 2005, Toronto, Ontario Canada

AIAA 2005-4931

Effects of Swirl Flow on an Atmospheric Inductively Coupled Plasma

Takayoshi Inoue [*], Makoto Matsui.[†], Hiroki Takayanagi.[‡], Kimiya Komurasaki [§] and Yoshihiro Arakawa [**]

University of Tokyo, Bunkyo-ku, Tokyo, 113-8656, JAPAN

An atmospheric inductively coupled plasma is expected to be used in the development of the thermal protection system for Venus missions. In this study effects of the swirl flow injection on the characteristics of an atmospheric ICP generator were investigated. The total enthalpy was measured by two ways; the sonic flow method and calorimetric method. A diode laser absorption spectroscopy was also applied to the measurement of the temperature and velocity of an extracted plume. The stagnation pressure was about 60 kPa and the work gas was argon. The experimental found that the specific enthalpy increased with decreasing the swirl flow fraction. This seems to arise from the change in the shape and the flow pattern inside the plasmas.

Nomenclature

A^*	=	cross section of the supersonic nozzle throat
α	=	swirl flow fraction defined as eq. (1)
c_p	=	specific heat
$\Delta\lambda_D$, $\Delta\lambda_P$	=	FWHM of the Doppler broadening and the resonance broadening
f_r	=	oscillator strength of the resonance transition
g_i, g_k	=	degeneracy of the lower state and the upper state
h_0	=	total enthalpy
h^*	=	static enthalpy at the Mach number of 1
k	=	Boltzmann constant
λ_0	=	center wavelength of the absorption profile
λ_r	=	wavelength of the resonance transition
$\dot{m}$	=	mass flow rate
M	=	mass of the probed particle
N_g	=	ground state number density of the target atom
p_0	=	stagnation pressure
R	=	gas constant
ρ_0	=	density at the stagnation point
ρ^*	=	density at the Mach number of 1
T	=	temperature
T_0	=	stagnation temperature
V	=	flow velocity

[*] Graduate student, JSPS Research Fellow, Department of Aeronautics and Astronautics, University of Tokyo, 7-3-1 Hongo, Bunkyo-ku, Tokyo, 113-8656, JAPAN, Student Member AIAA.
[†] JSPS Research Fellow, Department of Advanced Energy, University of Tokyo, 7-3-1 Hongo, Bunkyo-ku, Tokyo, 113-8656, JAPAN, Member AIAA.
[‡] Graduate student, Department of Aeronautics and Astronautics, University of Tokyo, 7-3-1 Hongo, Bunkyo-ku, Tokyo, 113-8656, JAPAN, Student Member AIAA.
[§] Associate Professor, Department of Advanced Energy, University of Tokyo, 7-3-1 Hongo, Bunkyo-ku, Tokyo, 113-8656, JAPAN, Member AIAA.
[**] Professor, Department of Aeronautics and Astronautics, University of Tokyo, 7-3-1 Hongo, Bunkyo-ku, Tokyo, 113-8656, JAPAN, Member AIAA.

I. Introduction

In 2002 the Solar System Exploration Decadal Survey (SSEDS) produced "New Frontiers in the Solar System: An Integrated Exploration Strategy", where they identified a broad range of science objectives and future missions for the next decade.[1] Some of the strategies of high priority are related with the compositional measurement of the surface and atmosphere of planets such as Mercury, Venus and so on. The most straightforward and reliable method should be in-situ probes and sample analysis by landers. A body of probe vehicle in a very high enthalpy atmospheric flow is protected by the Thermal Protection System (TPS). Any trouble of the TPS can lead to a fatal mission failure since the TPS is a single point-of failure sub system. The predicted entry heating environments for probes to Jupiter, Venus and Neptune are very severe with peak heat flux of several dozen kW/cm^2 and with stagnation pressure in the range from 0.1 MPa – 1.0 MPa. For these probes, the ablative TPS should be used, which amounted to 10 – 50 % of the probes in weight as was demonstrated in Galileo probe in 1995 and Pioneer probes in 1978.[2] Hence optimization of the TPS materials, its thickness and design will extend mission capability. Unfortunately it was pointed out that the TPS materials mounted in these missions should be re-qualified or may be unavailable.[3] Thereafter the development and sophisticated modeling of the TPS are significant issues and adequate ground test facilities have been needed.

Electrode-less inductively coupled plasmas (ICP) are expected to play an important role in the development of the thermal protection system (TPS) for Mars and Venus entry missions[4-7]. One of the most important features of the ICP is ability to operate under an atmosphere containing oxygen. Although some ICP wind tunnels have been developed to simulate the Mars entry environment with the pressure in the range from 1 kPa – 100 kPa[8], the stagnation pressure should be of more than atmospheric pressure for the Venus entry simulations. Usually ICP wind tunnels have employed swirl flow injection to stabilize the ICP generations. The role of the swirl flow becomes more important for higher-pressure operation.

Herdrich et.al. studied the effects on the flow enthalpy and tube heat loads under low pressure of about several torr.[9] They measured the flow enthalpy and tube cooling power with changing the fraction of the tangential and the axial mass flow rate and resulted that the tangential flow played an essential role in the term of the efficiency. On the other hand some papers reported that there were certain operational instabilities or operational limits, thereafter the tangential gas injection is thought to have a decisive significance for ICP generation, especially for higher pressure.[7,9,10] Yabuta et.al. evaluated the inlet design of an ICP torch with the static pressure of 1 atm.[11] Although, in their investigation, the ICP stability was characterized by the diameter of the inlet, their interests was directed to atomic emission spectrometry and how to reduce mass consumption of work gas, effect of the tangential flow on the performance in terms of high enthalpy flow generators was not studied. This work focuses on the effect of the swirl flow injection on characteristics of an atmospheric inductively coupled plasma and its super sonic jet. The total enthalpy of the heated flow and the flow parameters of the supersonic jet extracted from the atmospheric ICP were measured and effect of the swirl flow injection will be discussed.

II. Experimental Setup

A. ICP generator and RF power supply

Figure 1 shows a schematic diagram of an ICP generator. A quartz glass tube of 22 mm in the inner tube diameter as the plasma-sustaining channel was supported by a set of holders made of stainless steel, enabling generation of the ICP and observation of the plasma. A water-cooled load coil, fabricated from 3 mm copper tubing, has an inside diameter of 30 mm and consists of 5 turns. The coating of the copper tubing with a thermal shrinkage tube eliminated the problem of the short-circuiting between respective turns. RF power generator with oscillation frequency of 13.56 MHz and maximum output power of 1.25 kW was utilized and connected to a matching network through 50 Ω co-axial transmission line[12]. The matching network was controlled manually. The work gas was argon, with which the operations were stable under the current RF power levels.

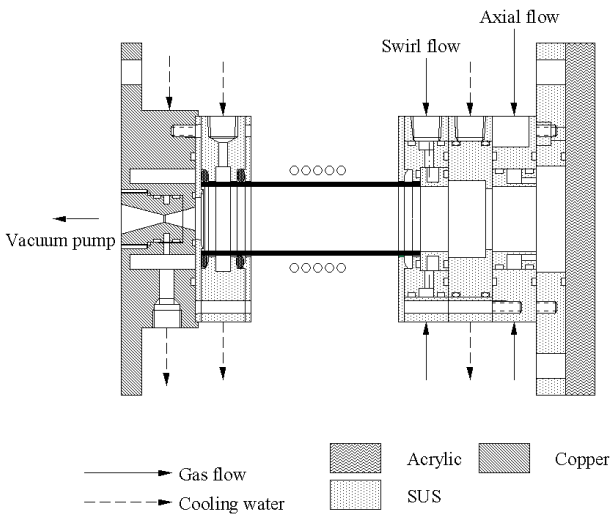

Figure 1. Schematic of the ICP generator.

B. Swirl flow injection

A tangential flow injection ring, which has two inlet bores of 1 mm-diameter, was used. An axial gas flow injection bore was also prepared in order investigate the effect of the swirl flow injection. The swirl flow fraction is defined as;

$$\alpha = \frac{\dot{m}_{swirl}}{\dot{m}_{total}} \tag{1}$$

where m_{swirll} : the mass flow rate of the swirl flow, m_{total} : the sum of the swirl mass flow rate and axial mass flow rate (fixed to 10 slm).

C. Supersonic nozzle

The ICP torch has a supersonic nozzle, of which the throat diameter is 2.4 mm and the expansion ratio is about 11 corresponding to Mach number of 4. The downstream of the nozzle was pumped out by two oil-sealed rotary pumps (total exhaust velocity: 80 m^3/h). In the following experimental the flow going through the nozzle was fixed to be 10 slm and the stagnation pressure of the flow was about 60 kPa and backpressure was about 200 Pa.

III. Measurement of Total enthalpy

A. Flow enthalpy measurements

In order to investigate effect of the swirl flow injection on the flow enthalpy, we employed two techniques; *sonic-flow method* and *calorimetric method*.

1. Sonic-flow method

The assumption that the heated flow up to the sonic point in the nozzle can be represented by an isentropic expansion is used to evaluate the total flow enthalpy by relating the mass flow rate and reservoir pressure to the enthalpy[13]. Winovich discussed extensively about validity of the method under some conditions. In our case we have to consider about the deviation from the assumption of calorically perfect gas and the effect of the boundary layer. The boundary layer would not cause significant deviation as long as the ratio of the flow temperature to the wall temperature being enough large, so the effect was neglected in this study. Generally the equation applicable to either a perfect or real gas flow is

$$\frac{\dot{m}}{A^* p_0} = \frac{\sqrt{2h_0}}{RT_0}\frac{\rho^*}{\rho_0}\left(1-\frac{h^*}{h_0}\right)^{1/2} \tag{1}$$

For calorically imperfect gas the specific heat is not constant so that eq. (1) should be numerically solved.

2. Calorimetric method

Calorimetric method is very simple one to evaluate the total enthalpy[14]. Schematic of a calorimeter used in this study is shown in figure 2. The flow channel wall was cooled by cooling water surrounding the channel, and the plasma flow exchange heat with the cooled wall. So the mass flow rate of the water and the increment in the temperature of the water provide the flow enthalpy. The following equation calculates the enthalpy. Of course it should be noted that incompleteness of the heat exchange results in the underestimation of the enthalpy.

$$h_0 = c_{p,water}\dot{m}_{water}\left(T_{out} - T_{in}\right) \tag{2}$$

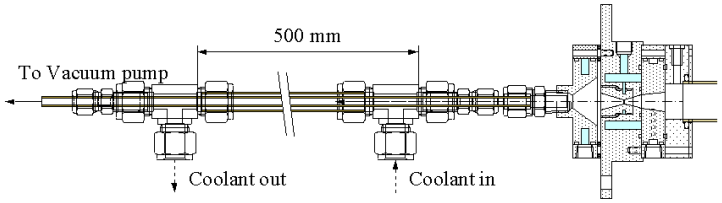

Figure.2 Heat exchanger with a double channel.

B. Experimental results

Averaged specific enthalpy was calculated by dividing the measured total enthalpy by mass flow rate (10slm). Figure 3 shows the experimental results. The figure confirmed the evident dependency on the swirl flow fraction. It can be seen that the specific enthalpy was increased with decreasing the swirl intensity. It should be noted that the estimated enthalpies from different methods deviated from each other with the increase in the RF power. The incompleteness of the heat exchange would be responsible for the deviation. Figure 4 shows the thermal efficiency defined as $\eta = h_0 / (P_{RF} - P_{coil})$, which does not contain the influence of the coupling between the coil and the plasma so that the substantial effect of the swirl flow from the aspect of hydrodynamics can be seen. The figure suggests that the thermal efficiency increased by a factor of 1.5 when the swirl flow fraction was decreased as possible and that was independent of RF power.

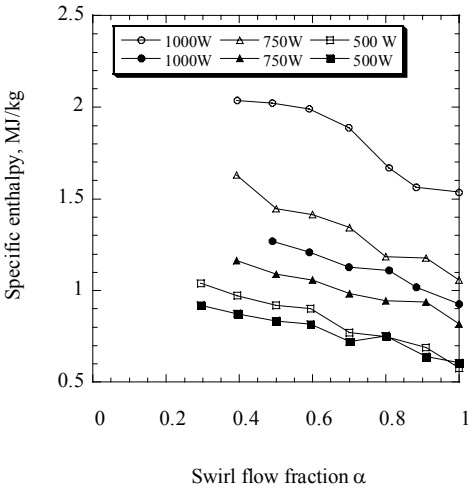

Figure 3 Measured specific enthalpy for various RF power input. The black and open dots represent the results obtained from sonic flow method and calorimetric method.

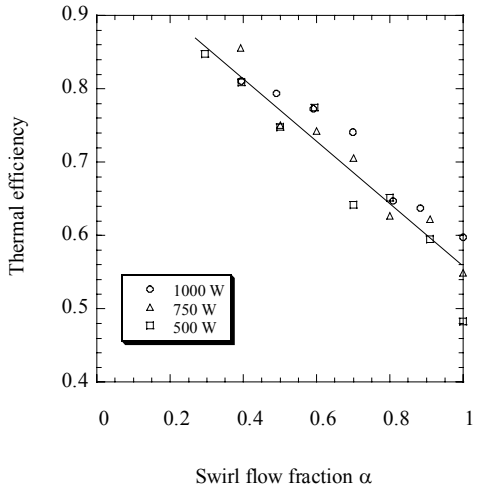

Figure 4 The thermal efficiency defined as $\eta = h_0 / (P_{RF} - P_{coil})$. P_{RF}: RF input power, P_{coil}: heat loss in the load coil.

IV. Diagnostics of Supersonic Jet by Laser Absorption Spectroscopy

In the preceding section the measurement of the averaged enthalpy of the ICPG was described. From the point of high-enthalpy flow generators the characteristics of the supersonic jet extracted from the ICPG are the most important ones. Here the non-intrusive measurement based on the Laser absorption spectroscopy (LAS) will be given. The RF power was to be 750 W throughout the spectroscopic study.

A. Laser Absorption Spectroscopy

In aerospace fields LAS using diode laser has been widely applied to the plume diagnostics in arc-jet researches and shock tunnel investigations. Matsui et.al. have applied LAS to some high-enthalpy flow generators; PWK3 (IRS), IPG3 (IRS), 20 kW-Arc-heater (JUTEM), and 1.2 kW-Arc-jet (University of Tokyo)[15].

One of the most important features of LAS is high resolution to identify the lineshape profiles. Narrow-bandwidth single-mode semiconductor laser enables to record detail lineshapes of the absorption profile. Although

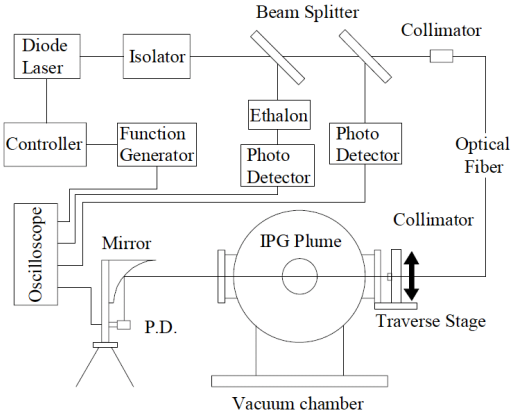

Figure 5 Schematic of a LAS system.

there are some techniques of wavelength modulation, a diode laser with external cavity was employed (EOSI DMD845) which is not accompanied with mode-hops in wide modulation width. Figure 5 shows a schematic of LAS system. There are three photodetectors; (A) measuring the absorption profile of the jet, (B) monitoring the absorption wavelength of the target line by using the reference discharge cell containing argon gas(0.9 torr), (C) obtaining the etalon signals. The target line was set to the atomic argon line of 4s ^{2}[3/2]^o → 4s ^{2}[5/2] (842.46 nm). The transition data of this line is shown in table 1.

Absorption profile of bound-bound transition line is broadened by various physical mechanisms, and is usually expressed by a convolution of the Gaussian distribution and the Lorentzian distributions. The dominant broadenings would be the Doppler broadening. For the transition the lower state has a resonant transition to the ground state so the resonant broadening should be considered. The broadening widths (FWHM) in SI units are expressed as follows[16,17];

$$\Delta\lambda_D = \left(\frac{8kT\ln 2}{Mc^2}\right)^{1/2}\lambda_0 \tag{3}$$

$$\Delta\lambda_R = 8.6\times10^4\left(\frac{g_i}{g_k}\right)^{1/2}\lambda^2\lambda_r f_r N_g \tag{4}$$

The Doppler broadening width is on the order of 1 pm. The specifications of the resonant transition from 4s ^{2}[3/2]^o to the ground state are also tabulated in table 1. The estimated line width of the resonance broadening was two orders of magnitude smaller than that of the Doppler broadening. Therefore the Doppler broadening was taken to be the dominant one and the line profiles were least-square fit to a Gaussian profile.

Table 1 Levels and transitions data of atomic argon.

Levels		
Configulation	Eneryg level, eV	Degeneracy
Ground state	0	1
4s 2[3/2]o	11.624	3
4s 2[5/2]	13.095	5

Transitions		
Transition	Wavelength, nm	Oscillator strength
Ground - 4s 2[3/2]o	106.66	6.09 e-2
4s 2[3/2]o - 4s 2[5/2]	842.46	0.381

B. Data analysis

Example raw data trace is shown in figure 6, which shows that the absorption by the plasma jet was very weak and signal to noise ratio was small. In order to obtain more accurate absorption profile, the profiles were averaged over 9 scans. Figure 7 shows the averaged absorption profile and its Gaussian fit in case of the swirl flow fraction of 0.5. The Gaussian fit based on the least-square-fit provided the Doppler broadening width and enabled to estimate the temperature by using eq.(1). Although, in order to know exact temperature distribution across the supersonic jet, we need to obtain absorption profiles across the jet and to compute the Abel deconvolution, the weak absorption made it difficult so the spatially resolved measurement was not conducted in this study. The averaged absorption profile would give smaller temperature than the local actual temperature on the axis to some extent.

The original laser power was assumed to vary linearly with time and the fit function was taken to be superposition of the Gaussian function and linear function;

$$\phi(\nu) = A\nu + B + \frac{C}{\pi^{1/2}\Delta\nu}\exp\left[-\left(\frac{\nu-\nu_0}{\Delta\nu}\right)^2\right] \tag{5}$$

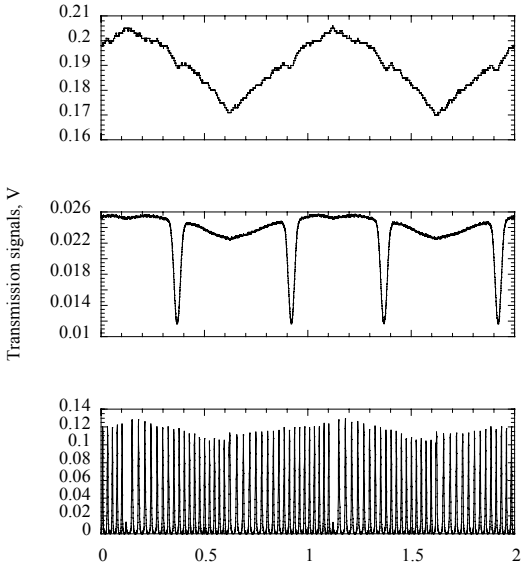

Figure 6 Example raw data showing repeated scans.(a) Supersonic jet absorption profile, (b) absorption profile of discharge cell, (c) a fixed etalon (0.75 GHz).

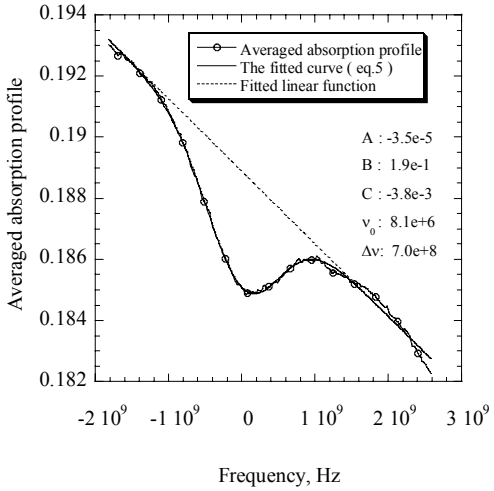

Figure7 Averaged absorption profile over 9 scans, and its fitted curve defined as eq. (5).

Figure 7 shows also the fitted curve of eq. (5) and its parameters. The FWHM of the Doppler broadening is expressed as $2(\ln 2)^{1/2}\Delta\nu$ and the broadening width in the wavelength is estimated to be about 2.8 pm in case of the swirl flow fraction of 0.5.

The flow velocity was determined from the Doppler shift measurement by LAS. The flow velocity is obtained by using the following equation;

$$V = \frac{\lambda_0}{\cos\theta}\Delta\nu_{shift} \tag{6}$$

where θ is the angle between the flow direction and the probe beam.. In the present setup α was about 74 deg.

C. Effect of swirl flow intensity on temperature and flow velocity

A CCD image of the supersonic jet is shown in figure 8 with an indication of the measurement point. The probe position was chosen so as to obtain larger absorption as possible because of the large transition probability from the target level to the ground state decreasing the number density of the target level with distance drastically. The measured temperatures are tabulated in table 2. The experimental result suggests that the smaller swirl flow fraction, the larger the temperature of the jet was.

Figure 9 shows the example data of the shift measurement. As to the shift measurement the probe position should be 25 mm-downstream from the position of the temperature measurements so that the signal-noise ratio was rather small. Hence, at the present configuration, the velocity was determined only for the case of the swirl flow fraction of 0.5. The measured shift of 0.5 GHz estimates the flow velocity to be 1.5×10^3 m/s.

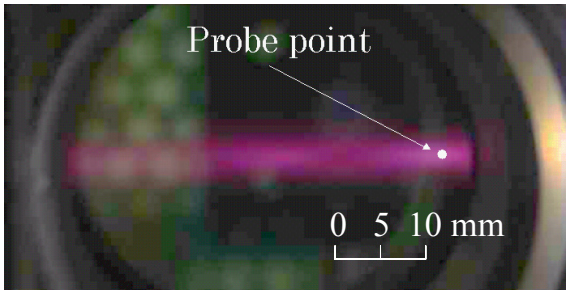

Figure 8 Photograph of the extracted plume.

Table. 2 Measured temperature and its error. "*" denotes "undetectable".

Swirl flow fraction	Temperature, K	Error in the Gaussian fit, %
1	*	*
0.9	*	*
0.8	441	7.0
0.7	730	3.0
0.6	664	1.5
0.5	836	1.6

Table. 3 Comparison of the estimated enthalpy from spectroscopic study and sonic flow method. The values are in MJ/kg.

h_{static}	$h_{kinetic}$	h_{total}	$h_{average}$
0.44	1.13	1.56	1.45

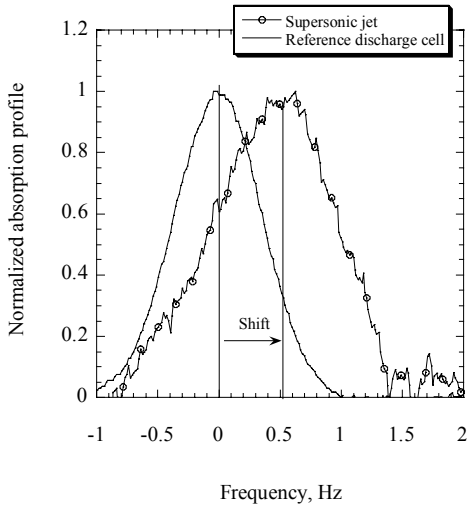

Figure 9 Example data of the shift measusment.

Only for the case of the swirl fraction of 0.5, the total enthalpy of the jet can be obtained from the measurement of the temperature and the velocity. Table 3 shows the comparison of the enthalpy estimated from the spectroscopic study and that obtained by the sonic flow method. The spectroscopic study estimates the total enthalpy, that is the sum of the static enthalpy and the kinetic enthalpy, to be about 1.6 MJ/kg, which agrees well with the result of the sonic flow method.

V. Discussion

A. CCD observations

CCD observations shown in figure 10 provide some ideas to discuss the effect of swirl flow. The images observe that the plasma shape and the generated position were significantly affected by the swirl flow fraction. In case of larger α the inductively heated region spread toward swirl injection head and formed longer shape. As some researchers described the swirl flow makes the pressure on the axis small. Since the discharge tends to be sustained in the smaller pressure region within the experimental conditions, the plasma was spread upstream.

In the heated region, the applied magnetic field induces the Lorenz force toward outward of the load coil because of the line of force inclining to the axis. In case of $\alpha = 1$ where the heated region spread toward upstream, the Lorenz force acts toward also upstream. This force would form vortex flow pattern with the effect of the swirl flow so that the temperature of the cold flow surrounding the ICP become large, resulting larger conductive loss to tube wall. On the contrary, in case of smaller α, the heated region existed in the downstream so that the Lorenz force was toward also downstream, that would bring the high-temperature plasma flow to the nozzle efficiently.

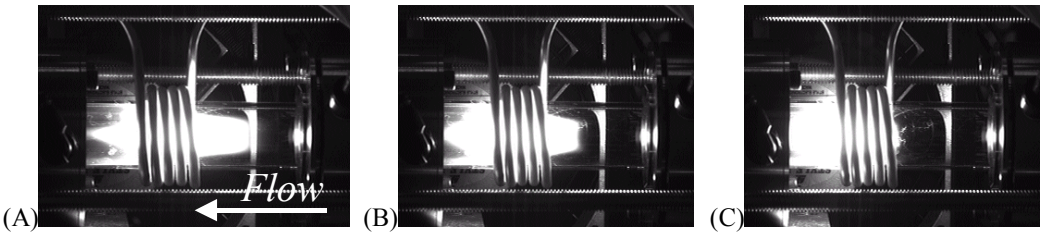

Figure 10 CCD images of ICPs for different swirl flow fraction; (A) α=1, (B) α=0.6, (C) α=0.23.

B. Higher pressure operations

In the preceding descriptions only the result of the case using 2.4 mm throat was mentioned. We have tried smaller throat diameter and larger mass flow rate in order to increase the stagnation pressure, but the thermal efficiency decreased, resulting the temperature measurements of the extracted jets having failed. This is because the higher-pressure operation is accompanied with larger recombination radiation loss. Additionally small diameter of

the throat makes the flow velocity slow and the enthalpy would be lost further by radiation. This can be also seen the following comparison; in a research on a ICP high-enthalpy generator in IRS using oxygen under the pressure of about several torr, they fed the power equivalent to 30 MJ/kg and obtained the flow of 27 MJ/kg[18]. In our case, where the stagnation pressure being two orders of magnitude larger than that of IRS, the input power of 2.5 MJ/kg produced the flow of which enthalpy was about 1.5 MJ/kg.

Obviously we have to decrease the mass flow rate to achieve the enthalpy level demanded for the Venus entry simulations with the RF power source of 1 kW. However instable behaviors of ICPs at low mass flow rate has been observed especially for higher-pressure operations[12]. This is the next issue to overcome.

VI. Summary

- Effects of the swirl flow injection on the characteristics of an atmospheric ICP generator were investigated.
- The averaged enthalpy and local enthalpy of the extracted plume increased by a factor of 1.5 with decreasing the swirl flow fraction.
- The swirl flow affected the shape and the position of the plasma significantly, which seem to be responsible for the thermal efficiency.

Acknowledgement

This work has been supported partially by the Ministry of Education, Science, Sports and Culture, Grant-in-Aid for Exploratory Research, and Research Fellowships of the Japan Society for the Promotion of Science for Young Scientists.

References

[1]Solar System Exploration Survey Space Studies Board, "New Frontiers in the Solar System: An Integrated Exploration Strategy," THE NATIONAL ACADEMIES PRESS, Washington DC, 2003.

[2]Seiff, A., et. al., "Measurements of Thermal Structure and Thermal Contrasts in the Atmosphere of Venus and Related Dynamical Observations: Results From the Four Pioneer Venus Probes" *J. Geophysical Research*, Vol. 85, No. A13, 1980, pp. 7909-7933.

[3]Laub, B., and Venkatapathy, E., "Thermal Protection System Technology and Facility Needs for Demanding Future Planetary Missions," Proceedings of the International Workshop on Planetary Probe Atmospheric Entry and Descent Trajectory Analysis and Science, I - 6.1 , Lisbon, Portugal, 2003.

[4]Bottin, B., Paris, S., Van Der Haegen, V., and Carbonaro, M., "Experimental and Computational Determination of the VKI Plasmatron Operating Envelope" *AIAA*-1999-3607.

[5]Herdrich, G., Auweter-Kurtz, M., and Endlich, P., "Mars Reentry Simulation Using the Inductively Heated Plasma Generator IPG4" *AIAA*-2001-31427.

[6]Ito, T., et.al., "Heating Tests of TPS samples in 110 kW ICP-heated wind tunnel," Proceedings of the 24th International Symposium on Space Technology and Science, 2004-e-20 , Miyazaki, Japan, 2004.

[7]Yamada, T., and Inatani, Y., "Inductively-coupled High Enthalpy Flow Generator for Planetary Entry Probes," Proceedings of the 24th International Symposium on Space Technology and Science, 2004-e-21 , Miyazaki, Japan, 2004.

[8]Smith, R.K., Wagner, D.A., and Cunningham, J.W., "A SURVEY OF CURRENT AND FUTURE PLASMA ARC-HEATED TEST FACILITIES FOR AEROSPACE AND COMMERCIAL APPLICATIONS" *AIAA*-1998-0146.

[9]Herdrich, G., Auweter-Kurtz, M., and Kurtz, H., Laux, T., Schreiber, E., "Investigation of the Inductively Heated Plasmagenerator IPG3 Using Injection Rings of Different Geometries" *AIAA*-2000-2445.

[10]Ito, T., et.al., "Heating Tests of TPS samples in 110 kW ICP-heated wind tunnel," Proceedings of the 24th International Symposium on Space Technology and Science, 2004-e-20 , Miyazaki, Japan, 2004.

[11]Yabuta, H., Miyahara, H., Watanabe, M., Hotta, E., and Okino, A., "Design and evaluation of dual inlet ICP torch for low gas consumption," *Journal of Analytical Atomic Spectrometry*, Vol.17, 2002, pp.1090–1095.

[12]Inoue, T., Uehara, S., Komurasaki, K., and Arakawa, Y., "Inductively Coupled Plasmas Supported by Laser Plasmas for High Enthalpy Flow" *AIAA*-2005-950.

[13]Winovich, W., "ON THE EQUILIBRIUM SONIC-FLOW METHOD FOR EVALUATING ELECTRIC-ARC AIR-HEATER PERFORMANCE," NASA-TN D-2132, 1964.

[14]Herdrich, G., Auweter-Kurtz, M., and Kurtz, H., "Operational Behavior of Inductively Heated Plasma Source IPG3 for Entry Simulations" *Journal of Thermophysics and Heat Transfer*, Vol. 16, No. 3, 2002, pp. 440-449.

[15]Matsui, M., Takayanagi, H., Oda, Y., Komurasaki, K., and Arakawa, Y., "Performance of arcjet-type atomic-oxygen generator by laser absorption spectroscopy and CFD analysis," *Vacuum*, Vol. 73, No. 3-4, 2004, pp. 341-346.

[16]Griem, H.R., Plasma Spectroscopy, McGraw-Hill, New York, 1964, Chap. 4.

[17]Drake, G.W.F., Atomic Molecular, & Optical Physics HANDBOOK, AIP, New York, 1996, Chap. 10.

[18]Matsui, M., Herdrich, G., Auweter-Kurutz, M., Komurasaki, K., and Arakawa, Y., "Laser Absorption Spectroscopy in Inductive Plasma Generator Flows" *AIAA*-2004-1222.